Environmental Science Nano

Displacement Reactions Between Environmentally and Biologically Relevant Ligands on TiO2 Nanoparticles: Insights into the Aging of Nanoparticles in the Environment

Journal:	*Environmental Science: Nano*
Manuscript ID	EN-ART-07-2018-000780.R3
Article Type:	Paper
Date Submitted by the Author:	19-Dec-2018
Complete List of Authors:	Wu, Haibin; University of California San Diego, Department of Chemistry and Biocheistry Gonzalez Pech, Natalia; University of California San Diego, Grassian, Vicki; University of California San Diego,

Environmental Significance. Wide spread usage of metal oxide nanoparticles causes some concern due to their potential risks once they get into the environment. Once nanoparticles are released in the environment they can undergo different aging and transformation processes which can significantly influence their surface composition which will impact other physicochemical properties as well as their interactions with organisms. Herein we investigate the details of the surface chemistry of humic acid on TiO_2 surfaces pre-coated with other environmentally and biologically relevant ligands in order to better understand how aging and transformation processes occur in the environment. Our results show that humic acid can displace more weakly bound molecules but for larger biological molecules such as strongly bound proteins, there is no displacement. Furthermore, nanoparticle suspensions are found to be stabilized by humic acid regardless of the original coating.

Displacement Reactions Between Environmentally and Biologically Relevant Ligands on TiO_2 Nanoparticles: Insights into the Aging of Nanoparticles in the Environment

Haibin Wu,[1] Natalia I. Gonzalez–Pech,[1] Vicki H. Grassian[1,2*]

[1]Department of Chemistry & Biochemistry, University of California San Diego, La Jolla, CA 92093, United States

[2]Departments of Nanoengineering and Scripps Institution of Oceanography, University of California San Diego, La Jolla, CA 92093, United States

[*]To whom correspondence should be addressed: vhgrassian@ucsd.edu

Abstract

Coatings on nanoparticle (NP) surfaces play a key role in dictating their behavior in the environment. For metal oxide NPs, the physicochemical processes of dissolution, aggregation, and reactivity are all impacted by surface coatings. The current study focuses on adsorption and displacement reactions of different molecular and biological species representative of different coatings on TiO_2 NP surfaces. These different species include ascorbic acid (AA), citric acid (CA), humic acid (HA) and bovine serum albumin (BSA) protein. Surface adsorption, desorption, and displacement reactions of these four species on 20 nm TiO_2 NPs were investigated using attenuated total reflectance–Fourier transform infrared spectroscopy. Further insights of these reactions and on the behavior of TiO_2 with these coatings were gained from quartz crystal microbalance with dissipation measurements, dynamic light scattering and sedimentation studies to investigate nanoparticle stability. Our results show that HA adsorbs strongly onto TiO_2 NP surfaces at neutral pH. In contrast, smaller acidic molecules such as AA and CA bind more weakly and, as a result, HA can displace these molecules from the TiO_2 surface as determined by two-dimensional correlation spectroscopy. In the case of BSA, HA does not displace the protein but instead co-adsorbs on the nanoparticle surface. Our results show that the relative binding affinity to the surface depends on the ability of different functional groups to interact with the surface and through non-specific surface interactions that become important for larger species with higher molar mass. To our knowledge, this is the first time that these types of displacement reactions on TiO_2 NPs have been investigated and probed with *in situ* techniques. The insights that this work provide are of relevance in understanding the fate of nanomaterials as ligand displacement reactions will modify the stability of these nanoparticles during their transport in the environment, nanoparticle agglomeration and their interactions with biological systems.

Introduction

Metal oxide nanomaterials and their composites have been extensively studied and developed, due to their vast potential applications as photocatalysts,[1-2] solar cells,[3] biosensors,[4] diagnostic,[5] and drug delivery.[6-7] Because of these developments, it is expected that these nanomaterials will be released into the environment.[8] Once in the environment, nanomaterials will undergo a variety of different aging and transformation processes, involving reactivity, dissolution, and both hetero- and homo- agglomeration, thus altering the properties of the nanomaterials over time.[9-14] Among various metal oxide nanomaterials, TiO_2-based products are some of the most widely used,[15] due to their unique photocatalytic properties[16-18] and biocompatibility.[19-23] However, modeling studies have indicated that an increased concentration of nanomaterials in the environment can create potential risks to various organisms.[24-27] Therefore, the fate of TiO_2 NPs in the environment has attracted much attention over the past decade. Several factors play a role in the fate of nanomaterials with the surface being an important one due to surface functionalization and surface ligand reactions.[28-31]

Natural organic matter (NOM) is expected to adsorb onto TiO_2 NPs released into the environment, and impact their agglomeration and stability,[32-36] thus affecting the mobility of TiO_2 NPs.[37] Humic acid (HA) is used as a typical model for NOM as it is widely distributed in soil, sediments, and water in the environment with concentrations that vary from 0.1 to 50 mg/L.[38] HA refers to a category of natural substances derived from the decomposition of plants and animals. HA is a collection of large macromolecular structures with high aromatic conjugated structures containing amino, hydroxyl, ketone, phenolic, and carboxylic functional groups.[39] Previous studies of metal-HA interactions show that HA can bind metal ions.[40-41] Among the different interaction mechanisms by which NOM adsorbs on NPs, surface ligand exchange between NP surface and a

variety of groups of NOM is the dominant interaction.[42] This interaction has two main steps:[43] (1) the outer-sphere complexation between polar functional groups and surface hydroxyl group, and (2) the ligand exchange resulting in formation of an inner-sphere complex. The spectroscopic studies suggest that the adsorption of HA on TiO_2 NPs involves various functional groups, such as phenol and carboxyl groups.[44-45] In addition, the adsorption process is significantly modified by the pH: the hydroxyl groups on the surface are protonated favoring ligand exchange.[42, 44] Furthermore, studies have shown that interactions between NOM or HA have significant impacts on the properties of NPs, such as chemical reactivity,[46-47] dissolution,[48] and toxicity.[49] HA as a surface ligand can significantly influence the fate and properties of nanomaterials in the environment.

Attenuated total reflectance–Fourier transform infrared (ATR-FTIR) spectroscopy allows the *in situ* monitoring of adsorbed species by measuring spectral changes during the adsorption of ligands onto surfaces. Although adsorption of ligands on nanomaterials has been intensively studied by this technique,[44, 50-55] most of these studies focus on the adsorption processes on hydroxylated TiO_2 NPs surface. However, TiO_2 NPs are often coated by ligands because surfactants and surface ligands are used in the wet chemical synthesis of nanomaterials. As such, it is expected that the released TiO_2 NPs in the environment undergo diverse surface ligand reactions, especially ligand displacement reactions. It is crucial to understand the displacement reactions that TiO_2 NPs may undergo in the environment, since surface coatings can significantly affect the physiochemical properties. Nevertheless, there are few reports about mechanisms of displacement reactions and the impact of these reactions on the fate of TiO_2 NPs. Herein, ATR-FTIR spectroscopy is used to explore the mechanism of displacement reactions between environmentally and biologically relevant ligands including ascorbic acid (AA), citric acid (CA),

and bovine serum albumin (BSA) by HA. AA and CA were selected due to their common use as molecular coatings.[56] Moreover, they are also found in various biologically relevant systems with different concentrations (e.g. 0.1 mM CA in blood plasma[52] and 40 – 770 mg/kg AA in fruits[57]). BSA is used as a model of human serum albumin (typical concentration in blood is 3.5-5 g/dL)[58] and other proteins that NPs interact with in the environment.[59] In order to get a better understanding of the effect of NOM on TiO_2 NPs in the environment, HA is chosen as a model to show how NOM displacement reactions may impact NP surfaces and NP sedimentation behavior.

Experimental Methods

ATR-FTIR Spectroscopy. ATR-FTIR spectra were recorded using a 500 μl horizontal ATR flow cell with an AMTIR window (Pike Technologies Inc.) in a Nicolet iS 10 FTIR spectrometer equipped with an MCT-A detector. Spectra were collected with 264 scans at an instrument resolution of 4 cm^{-1} in the AMTIR window range (750 to 4000 cm^{-1}). In order to control pH, all solutions were prepared by dissolving the corresponding solutes (e.g. AA, CA, HA, and BSA) in 25 mM 4-(2-hydroxyethyl)-1-piperazineethanesulfonic acid (HEPES, Fisher Scientific) buffered solutions. Unless otherwise indicated, all solutions contain HEPES to maintain a pH of 7.5.

Solution phase spectra were collected for 100 mM citric acid (CA), 100 mM ascorbic acid (AA), 10 g/L bovine serum albumin (BSA) and 1 g/L humic acid (HA). For these adsorption studies, the following concentrations were used: 10 mM AA, 10 mM CA, 1 g/L BSA, and 0.05 g/L HA solutions. The adsorption studies were carried out by flowing solutions over TiO_2 NP thin films at a fixed flow rate (~ 0.4 mL/min). The morphology and crystalline phase of TiO_2 NPs are shown in Electronic Supplementary Information Figure S1, indicating that TiO_2 NPs have an average size of 23 ± 8 nm and their crystalline in nature containing mostly anatase with a small

amount of rutile. The thin film was prepared by drying 1 mL of 1 g/L TiO_2 NPs on AMTIR crystal overnight (Figure S2). After the adsorption study, the HA solution (0.05 g/L) was immediately introduced to the same TiO_2 NP thin film for the displacement reaction. All spectra were recorded every five minutes to monitor the process. To avoid the interference from the buffer, the range below 1200 cm^{-1} was not included in the analysis as the HEPES buffer showed strong absorptions in this region.

Analysis of Two-Dimensional Correlation Spectroscopy. Two-dimensional correlation spectroscopy (2D-COS) is a well-established analytical method used to investigate changes that occur following an external perturbation e.g. time and pH.[45, 60] Furthermore, the sequential order of functional band intensity changes in the displacement process can be analyzed by synchronous and asynchronous maps of 2D-COS, thus revealing the mechanism of displacement processes involving HA on TiO_2 NPs first coated with other adsorbates. For the 2D-COS, pretreatments of data (e.g. baseline correction and smoothing) are recommended to avoid artificial peaks in 2D maps. The baseline correction was carried out by a simple offset and the smoothing function uses the Savitzky-Golay algorithm. All spectra used for 2D-COS were baseline corrected and smoothed using the OMNIC 9 software (Thermo Fisher). 2D-COS was performed on a set of dynamic ATR-FTIR spectra at intervals of 5 min collected during the displacement process. The computation of 2D-COS was performed by Matlab R 2017b (MathWorks Inc.) and 2dshige version 1.3 (Shigeaki Mortita, Kwansei-Gaukuin University, 2004-2005) following the algorithm developed by Noda.[61-62] The results in the synchronous (Φ) and asynchronous (Ψ) 2D correlation spectral maps can be interpreted as follows, which is also known as Noda's rules.[63] In the synchronous map, a positive value of cross peaks indicates the change of corresponding spectral variations either increase or decrease in the same direction with the applied external perturbation, whereas a negative value

means the changes in two opposite directions: one increases and the other decreases. The sequential order between the two bands $\boldsymbol{\upsilon_1}$ and $\boldsymbol{\upsilon_2}$ can be determined by the signs of synchronous and asynchronous correlation maps: if the signs of $\boldsymbol{\Phi}$ and $\boldsymbol{\Psi}$ are the same, the change of $\boldsymbol{\upsilon_1}$band occurs before the $\boldsymbol{\upsilon_2}$ band and if the signs are opposite, the change of $\boldsymbol{\upsilon_1}$ band occurs after the $\boldsymbol{\upsilon_2}$ band. A zero value suggests the two bands have no correlation.

Quartz Crystal Microbalance with Dissipation (QCM-D). The adsorption behavior was also interrogated by a quartz crystal microbalance with dissipation (QSense Pro, Biolin Scientific) using a commercial TiO_2 coated 5 MHz AT-cut quartz sensors (Biolin Scientific, QSX 999). The TiO_2 sensors were custom made by Biolin Scientific and the provided characterization is shown in Figure S3. X-ray photoelectron spectroscopy confirms a Ti (IV) oxide. The presence of a shoulder at a binding energy around 532eV in Figure S3b indicates that the TiO_2 surface on the sensor is hydroxylated.[64] Frequency and energy dissipation changes were monitored as a function of time. The TiO_2 sensors were reused several times for different measurements. Between each measurement, the crystal sensors were cleaned by soaking in 2% sodium dodecyl sulfate solution (SDS, Sigma Aldrich), dried with N_2, and then treated in a UV-ozone chamber for 20 min. The baseline was collected with Milli-Q water. A gentle flow of each solution was maintained over the TiO_2 surface at a flow rate of 50 µL/min for 60 min. Following this, the flow was stopped, and the solution was kept over the surface for 30 min for equilibration. Reviakine *et al*. proposed a very strict criteria that the ratio of the change in dissipation to the change in frequency should be less than 4×10^{-7} Hz for a laterally homogeneous film in order to apply the Sauerbrey equation shown in Eq. 1.[65] The mass gain can still be calculated based on the Sauerbrey equation for the surface when there are small changes in dissipation less than 2 ppm,[66]

$$\Delta m = \frac{C\times\Delta F}{n} \qquad \text{Eq. 1, [67]}$$

where Δm is the mass gained per unit area (ng·cm^{-2}), ΔF is frequency shift (Hz^{-1}), C is a constant value of 17.7 ng·cm^{-2} ·Hz^{-1} for a 5 MHz AT-cut QCM sensor, and n the overtone number. Overtones 5, 7, 9 and 11 were monitored for all measurements. The QCM-D plots shown herein have all been normalized by the overtone number.

Sedimentation and Dynamic Light Scattering. The solutions for sedimentation and dynamic light scattering (DLS) studies were prepared by dispersing TiO_2 NP powder in 10 mM AA, 10 mM CA, and 1 g/L BSA solutions, respectively. The pH and ionic strength were kept at 7.5 and 0.03 M (87.6 mg NaCl in 50 mL). TiO_2 NP suspensions were sonicated for 10 min for mixing prior to placing on a Cole–Parmer rotator overnight. The concentrations of TiO_2 NP suspensions for sedimentation and DLS are 0.5 g/L and 0.1 g/L, respectively. An aliquot was used for the sedimentation and DLS analysis of pre-coated TiO_2 NPs. Then, for the displaced coating samples, 15 mL aliquots were transferred to 15 mL centrifuge tubes and then centrifuged at 10000 rpm for 20 min. After carefully removing the supernatant, 15 mL of 0.05g/L HA solution at same pH and ionic strength was added to the centrifuge tubes. The suspensions were sonicated for 10 min and mixed overnight. The samples were then used for the sedimentation and DLS analysis. The sedimentation experiments were performed using a UV–Vis spectrometer (Lambda 35, PerkinElmer), by monitoring the light intensity at a wavelength of 550 nm over time. The DLS measurement was conducted with a Delsa Nano C instrument (Beckman Coulter Inc.).

Results and Discussion

Adsorption of AA, CA, HA and BSA on TiO_2 NP Surfaces. Table 1 shows both molecular and representative structures of the relevant species under study, ascorbic acid (AA), citric acid (CA), humic acid (HA) and bovine serum albumin (BSA), along with information about the pH

dependent behavior, including pK_a values and the pH–dependent conformations in the case of BSA. The functional groups within each molecule are relevant for the adsorption on TiO_2 NPs, since the adsorption process often involves exchange reactions between molecules and the surface hydroxyl groups and or hydrogen bonding interactions. [42, 61-62, 68] The ATR-FTIR spectra shown in Figure 1 provide the details of the adsorption of AA, CA, HA and BSA onto TiO_2 surfaces by monitoring the vibrational frequencies and intensity of the functional groups. In addition, the solution phase spectra of these are also shown.

AA is the smallest molecular species amongst the four and its structure is composed of a primary OH, a secondary OH, and an enediol in a lactone. At pH 7.5, one of the enols in AA is deprotonated, and the deprotonation improves the conjugation enediol group and C=O. As seen in Figure 1a, the conjugation of the enediolate with the C=O bond causes a shift of the C=C stretching frequency to 1581 cm^{-1} in solution. However, when AA binds to the TiO_2 surface, there is a blue shift to 1590 cm^{-1}. The binding mode of AA on TiO_2 surface has been reported

Table 1. Representation of different molecules used in this study and their different pH dependent properties (protonation and secondary conformation).

AA	CA	HA	BSA
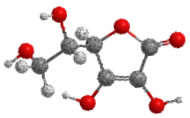	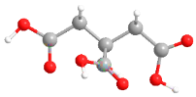	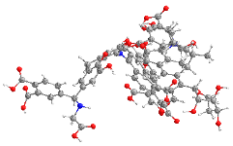	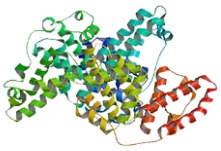
pK_a=4.2	pK_a=3.1	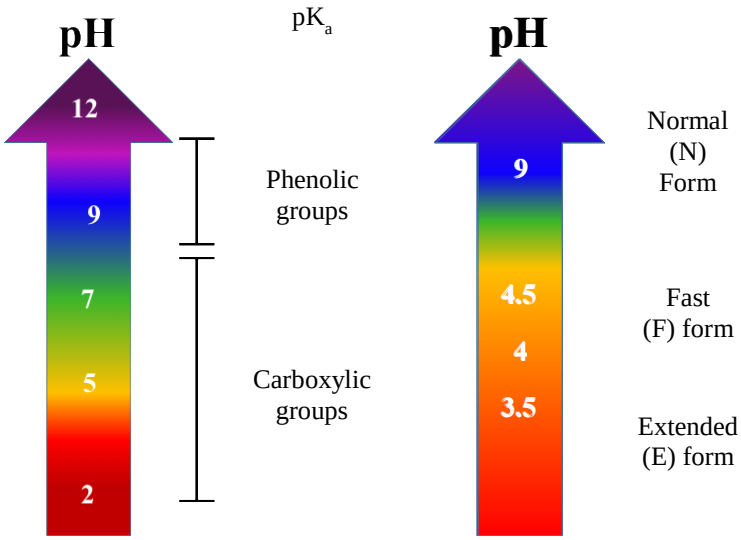	
$H_2Asc \rightleftarrows HAsc^-$	$H_3Cit \rightleftarrows H_2Cit^-$		
pK_a=11.8	pK_a= 4.76		
$HAsc^- \rightleftarrows Asc^{2-}$	$H_2Cit^- \rightleftarrows HCit^{2-}$		
	pK_a=5.8		

previously.[69] AA binds to Ti (IV) sites through the enediols. One enolate binds to Ti (IV) directly, and the other enol group assists in chelating to a Ti (IV) ion which then forms a five membered ring structure with Ti (IV) ion. This is supported by the shift in the vibration of C-O from 1356 to 1345 cm^{-1} during the adsorption. A charge transfer occurs between adsorbed AA and Ti (IV) ion.[69] In this structure, the lactone ring in AA is positively charged,[70-71] possibly resulting in a blue shift

of carbonyl vibration mode into from 1721 cm^{-1} and 1773 cm^{-1}. Besides, AA can also bind to Ti (IV) through only one enediolate, thus carbonyl vibration shifts from 1721 to 1711 cm^{-1}.

For CA, the structure consists of a tertiary alcohol OH and three carboxylic groups that are all deprotonated at pH 7.5.[52] The spectra for the free solution phase and adsorbed molecules are shown in Figure 1b. The asymmetric stretching vibration of the carboxylate groups is around 1570 cm^{-1} in both adsorption and solution spectra, but the symmetric vibration shifts from 1390 cm^{-1} in

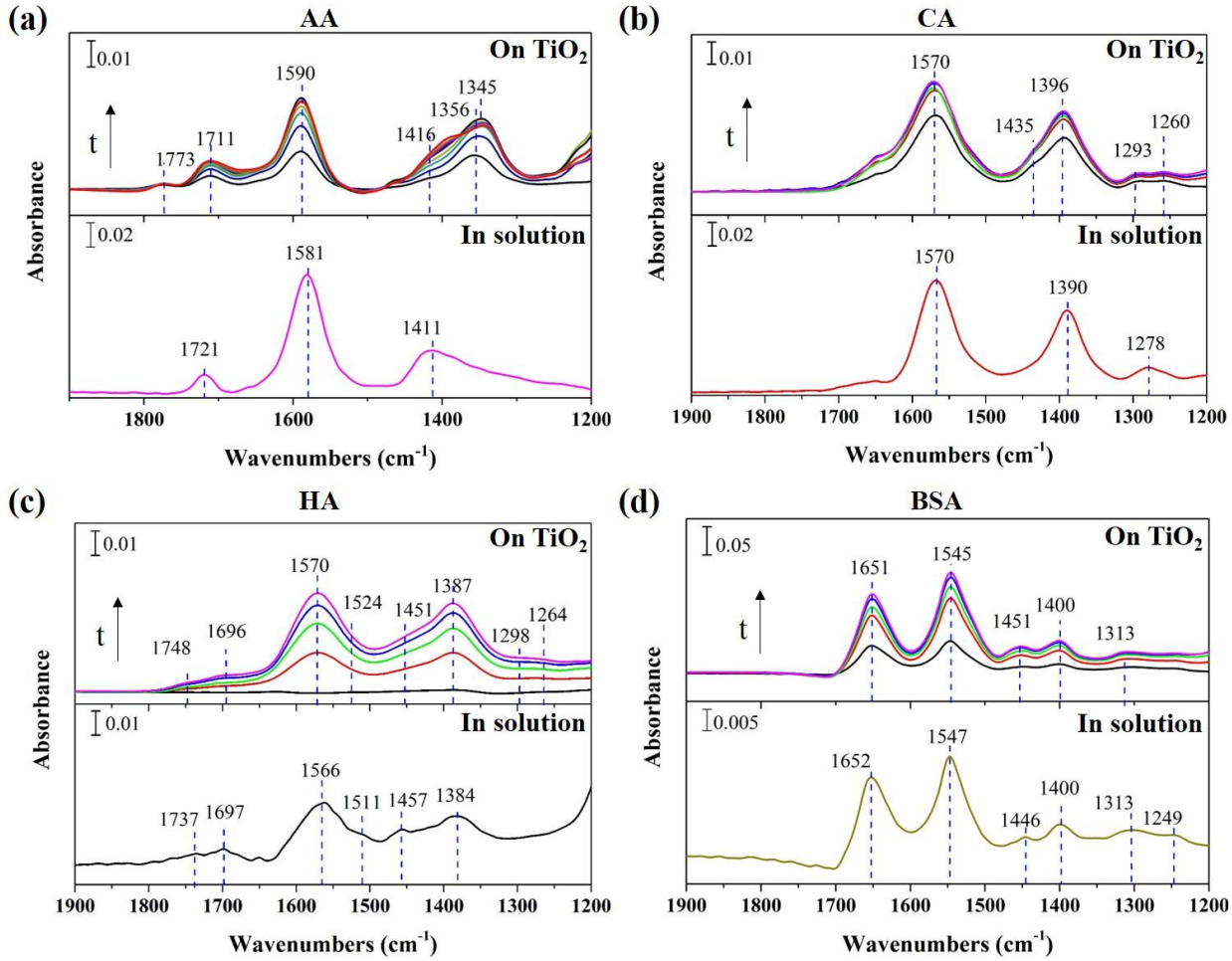

Figure 1. ATR–FTIR spectra of target species adsorbed onto TiO_2 and in solution phases. (a) Spectra of adsorbed 10 mM and in solution 100 mM AA; (b) spectra of adsorbed 10 mM and in solution 100 mM CA; (c) spectra of adsorbed 0.05 g/L and in solution 1 g/L HA; (d) spectra of adsorbed 1 g/L on and in solution 10 g/L BSA. The adsorption spectra shown were collected at 5 min (black), 30 min (red), 60 min (green), 90 (blue), 120 min (magenta).

Table 2. Assignments for the vibrational frequencies (cm^{-1}) of the main functional groups in the studied molecules.

molecule	vibrational mode	this work (cm^{-1})		literature (cm^{-1}) [44, 52, 69, 78-86]
		solution	adsorbed	
AA	υ (C=O)	1721	1773, 1711	1780, 1725, 1702
	υ (C=C)	1581	1590	1604, 1595,1594
	υ (enediolate, C-OH)	1411	1416	1415, 1345
	δ (C-OH) / δ (C-H)		1356	1396,1359,1369
	υ (enediolate, C-OH) *		1345	1345
CA	υ_{asym} (COO^-)	1570	1570	1580−1569
	υ_{sym} (COO-)/OH def	1390	1396, 1435	1436, 1400−1391
	δ(O=C-O-)	1278	1293, 1260	1292-1260
HA	υ (C=O)	1737, 1697	1748,1696	1720, 1640
	υ_{asym} (COO^-)	1566	1570	1590−1550
	υ (C=C)	1511	1524	1525
	δ (C-H)	1457	1451	1450
	υ_{sym} (COO-)/OH def	1384	1387	1350
	υ (phenol C-OH)		1264	1270
BSA	amide I υ_s (c=O) major + υ_s (C-N) minor	1652	1651	1695−1630
	amide II υ_s (C-N) +δ (N-H) out of phase	1547	1545	1550
	δ (C-H)	1446	1451	1500-1400
	amide III or υ (C-O)/ υ (C-O-C)/ υ (C-C)	1400, 1313, 1249	1400,1313	1400−1000

* the vibration frequency of enediolate forming a 5-membered ring.

solution to 1396 cm^{-1} when adsorbed on the TiO_2 NP surface and a shoulder appears at 1435 cm^{-1}. The splitting of carboxylate vibration between asymmetric and symmetric vibrations indicates that some carboxylates interact with surface through a bidentate bridging mode. It is worth noting that the band of the deformation O=C–O at 1278 cm^{-1} in solution phase shifts to higher wavenumbers at ~1293 cm^{-1} for adsorbed species on TiO_2 NPs. This is caused by a specific

interaction between COO^- and Ti (IV), suggestive of monodentate bonding. Park *et al.* propose that citrate binds on surface through bidentate bridging via the central carboxylate ion and monodentate via one of terminal carboxylates.[72]

HA has multiple functional groups that can participate in the interaction with TiO_2, including carbonyl, amide, carboxylate, phenol, polysaccharide, and alcohol hydroxyl.[44-45] In the spectra for adsorbed HA on TiO_2 NPs (Figure 1c), the dominant absorption bands appear at 1570 and 1387 cm^{-1}, which correspond to the asymmetric and symmetric carboxylate vibrations, respectively. Importantly, these characteristic frequencies shift from 1566 cm^{-1} and 1384 cm^{-1} in solution phase to 1570 cm^{-1} and 1386 cm^{-1} for adsorbed species, respectively. This indicates that HA binds to TiO_2 NP surface via carboxylate as suggested by others.[44] Other characteristic absorption bands including 1748 cm^{-1} for the C=O stretching of protonated carboxylic acid group, 1451 cm^{-1} for the C–H bending mode, and 1298 cm^{-1} for –COO–Ti groups are seen. In addition, an absorption at 1264 cm^{-1} possibly comes from the binding mode phenolic C–O–Ti, which is not present in solution phase.[73]

For BSA, the spectra (Figure 1d) show an amide I band at near 1650 cm^{-1}, which mainly consists of stretching vibration C=O of amide.[74] The other intense band in the spectra is due to the amide II band around 1550 cm^{-1} caused by the bending of N–H and C–N. In previous studies, we have observed information about the small changes in the secondary structures which include α–helixes, extended chains and turns during the adsorption of BSA onto TiO_2 NPs.[60, 75-77] A summary of these peak assignments are listed in Table 2, including comparison to the values reported in the literatures.[44, 52, 69, 78-86]

The adsorption-desorption process was also investigated by ATR-FTIR, shown in Figure 2. The desorption behavior of the adsorbed molecules when washing with a buffer solution reveals the nature of the interaction with the surface. This is observed when the maximum intensity reached during the adsorption process for AA and CA decreases upon the desorption process. In addition, Figure 2 shows that AA has a slower adsorption and desorption kinetics compared to CA. This discrepancy relates to the binding modes to TiO_2 surface. AA tends to form a 5-membered ring with Ti (IV) while CA binds via a simpler bidentate bridging mode. For BSA and HA, the intensity of adsorption spectra approaches the maximum values and its intensity does not change when buffer is introduced suggesting irreversible adsorption and little loss of BSA or HA from the

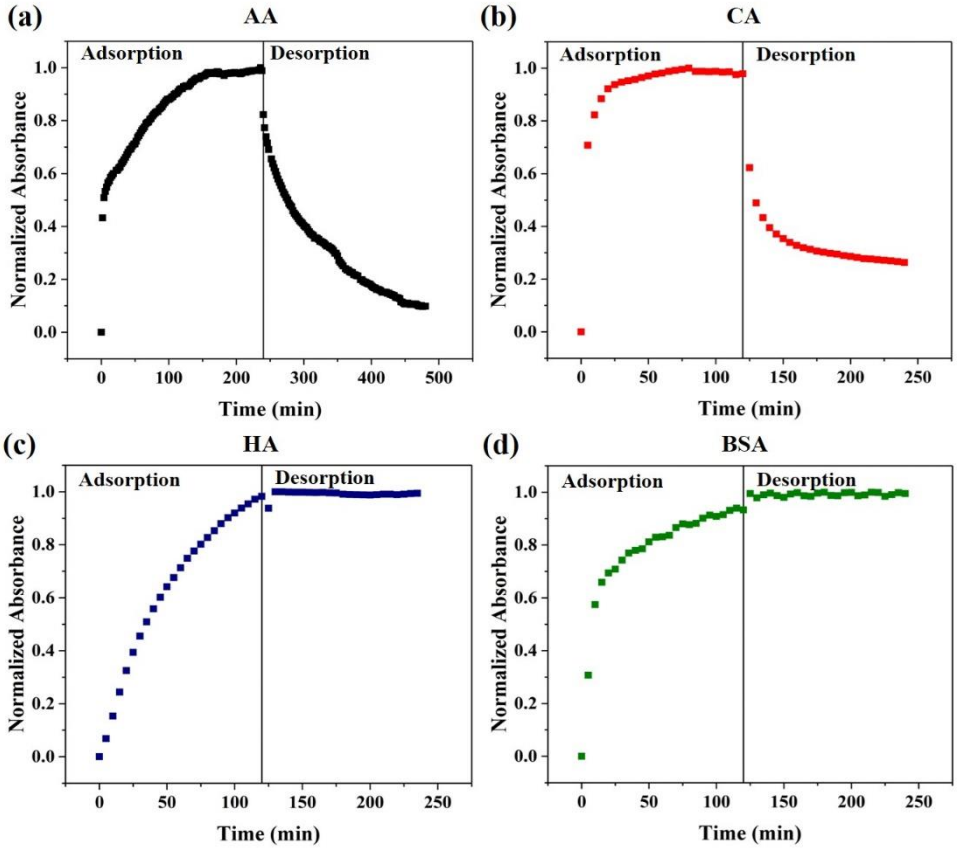

Figure 2. The adsorption and desorption processes of (a) 10 mM AA, (b) 10 mM CA, (c) 0.05 g/L HA and (d) 1 g/L BSA. The intensity was normalized using the absorbance at 1385 cm^{-1} for AA, 1570 cm^{-1} for CA, 1570 cm^{-1} for HA, and 1545 cm^{-1} for BSA, respectively.

surface. In contrast to AA and CA, macromolecules such as BSA and HA, prefer to adsorb on surface by forming monolayer e.g. BSA[83] and HA.[87]

Following these ATR-FTIR experiments, QCM-D was used to investigate adsorption and desorption processes of these four species by measuring the adsorbed mass and assessing conformation changes of the molecules by monitoring changes in frequency (ΔF) and dissipation (ΔD), respectively. Although the QCM experiment uses a deposited TiO_2 surface but not NPs, it is expected that these measurements can provide additional insights into the interactions of these

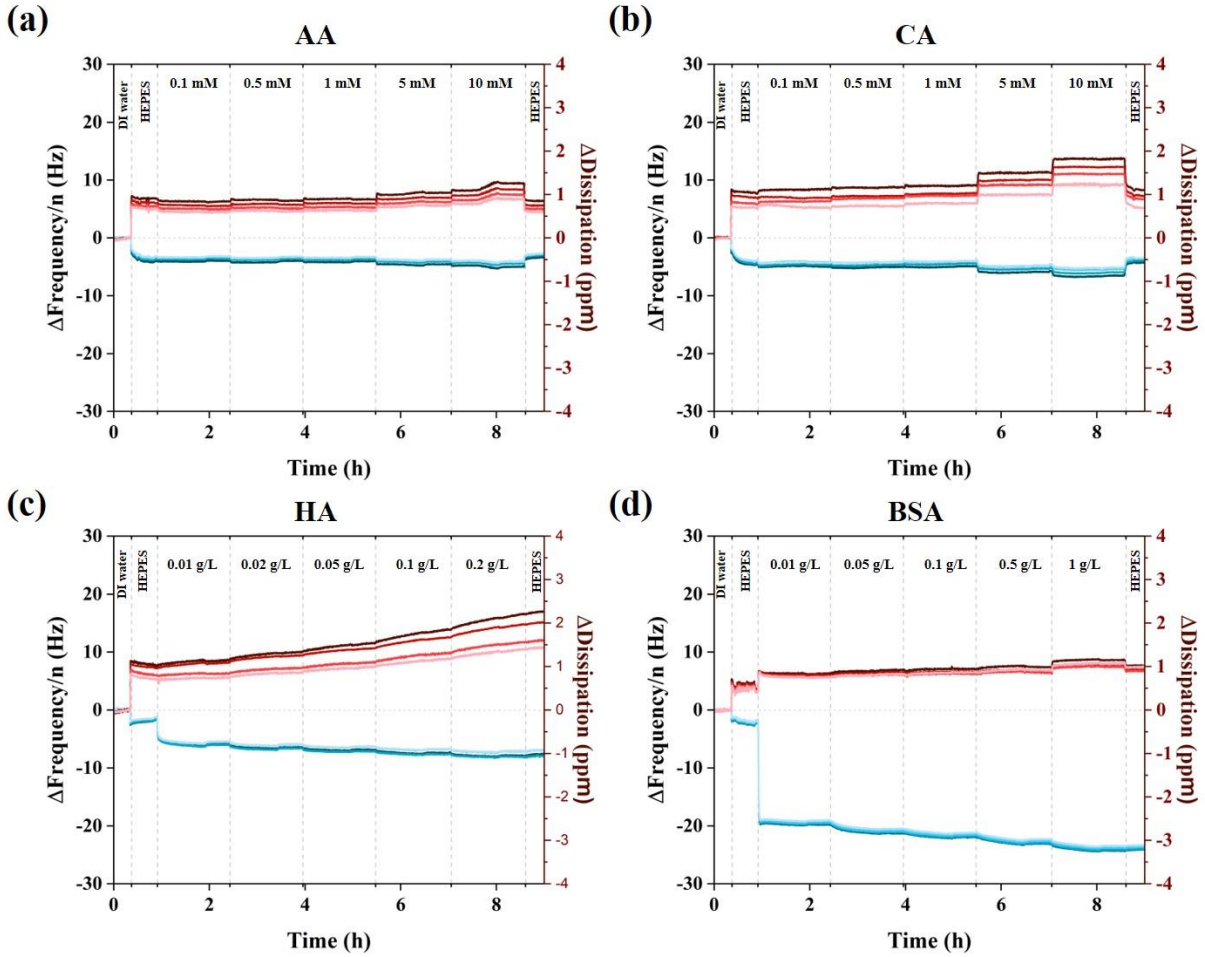

Figure 3. Shifts in frequency and dissipation, normalized by overtone number, for the adsorption of ascorbic acid (a), citric acid (b), humic acid (c) and bovine serum albumin (d) onto a TiO_2 coated surface with QCM–D. Blue and red lines represents changes in frequency and dissipation, respectively. Data are shown for overtones 5, 7, 9, and 11 in a color gradient, in which the darker colors are for smaller overtones.

Table 3. Summary of the surface coverage assuming a rigid layer.

AA		CA		BSA		HA	
Initial concentration, mM	**Adsorbed molecules (St. Dev.), x10^{13} molecules/cm^2**	**Initial concentration, mM**	**Adsorbed molecules (St. Dev.), x10^{13} molecules/cm^2**	**Initial concentration, g/L**	**Adsorbed molecules (St. Dev.), x10^{13} molecules/cm^2**	**Initial concentration, g/L**	**Adsorbed molecules (St. Dev.), x10^{13} molecules/cm^2**
0.10*	21.3 (2.06)	0.10*	25.4 (1.99)	0.01*	0.32 (0.01)	0.01*	1.57 (0.06)
0.50	21.5 (1.96)	0.50	25.1 (2.27)	0.05	0.34 (0.01)	0.02	1.71 (0.08)
1.00	21.8 (2.03)	1.00	24.3 (2.41)	0.10	0.35 (0.01)	0.05	1.81 (0.09)
5.00	24.8 (2.26)	5.00	28.9 (2.58)	0.50	0.37 (0.01)	0.10	1.95 (0.10)
10.0	27.0 (2.59)	10.0	33.0 (3.78)	1.00	0.39 (0.01)	0.20	2.07 (0.11)

* At this concentration, the adsorbed mass includes a contribution from HEPES

molecules with TiO_2 surfaces and thus complementing the ATR-FTIR measurements. It is important to note that the QCM will not consider the curvature effect on the adsorption onto NPs but can verify in a quantitative manner the qualitative observations from the ATR-FTIR. In particular, it will show if the surface is fully covered with the adsorbate at the concentration used in the ATR-FTIR experiments. The sensors are first exposed to the buffer solution, and a small amount of HEPES is adsorbed. Then, the corresponding adsorbate is introduced. Solutions with 5 increasing concentrations were introduced to calculate the surface coverage (Table 3, molecules/cm^2). However, due to the similarity in the molar mass, the displacement between HEPES and AA or CA on surface do not exhibit a discernible frequency shift at low concentrations. Thus, AA (Figure 3a) and CA (Figure 3b) gained mass, can be only associated to the adsorbate when concentrations are higher than 5 mM. As shown in Table 3, for the small molecules AA and CA with relatively weak interaction with the surface, the number of adsorbed molecules is not greatly affected at low solution concentrations (smaller than 5 mM), indicating at such

concentrations the small molecules form a stable interface like a monolayer. In contrast, a noticeable gain is observed at higher concentrations (larger than 5 mM), which is associated with an increase in dissipation. AA and CA have relatively weak interaction with the surface so that they are reversibly or partially reversibly adsorbed on the surface. However, this increase in mass and dissipation is diminished when the surface is washed with buffer solution. The removal of the loosely bonded molecules when flowing the buffer solution, is in good agreement with adsorption-desorption study by ATR-FTIR (Figure 2). In contrast, larger macromolecular species such as HA (Figure 3c) and a protein such as BSA (Figure 3d) show a significant decrease in ΔF at low concentrations that is far larger than that observed for the HEPES buffer solution. The surface coverage (molecules/cm^2) observed for the different concentrations of the analyzed solutions are summarized in Table 3.

For AA, CA, and BSA, the adsorption process at each condition would reach the equilibrium very quickly revealing that ΔD and ΔF quickly level off and become constant values. However, HA never exhibits a plateau phase in the ΔD plot which is different from other molecules, suggesting that HA alters its conformation in order to adsorb onto the TiO_2 surface. In addition, the shifts in dissipation provide insights into the viscoelasticity of the adhered layers.[65, 88-89] The change in dissipation (ΔD) relates to how much the added layer deforms (soft surface) and how much the added layer resists deformation (rigid surface) when the crystal shears.[90] A rigid surface, such as monolayer of adsorbed molecules, typically has a value of ΔD less than 1 ppm (10^{-6}), while values larger than 1 ppm imply a soft surface.[91] The discrepancy on the dissipation plots of the different overtones supports the formation of a softer film,[65, 89] which in the case of HA, suggests the changes on conformation is caused by intermolecular interactions and by the different

adsorption modes generated for the multiple functional groups in the macromolecule, which is in a good agreement with the ATR-FTIR results.

Displacement Reactions. In these experiments, the displacement process was recorded by

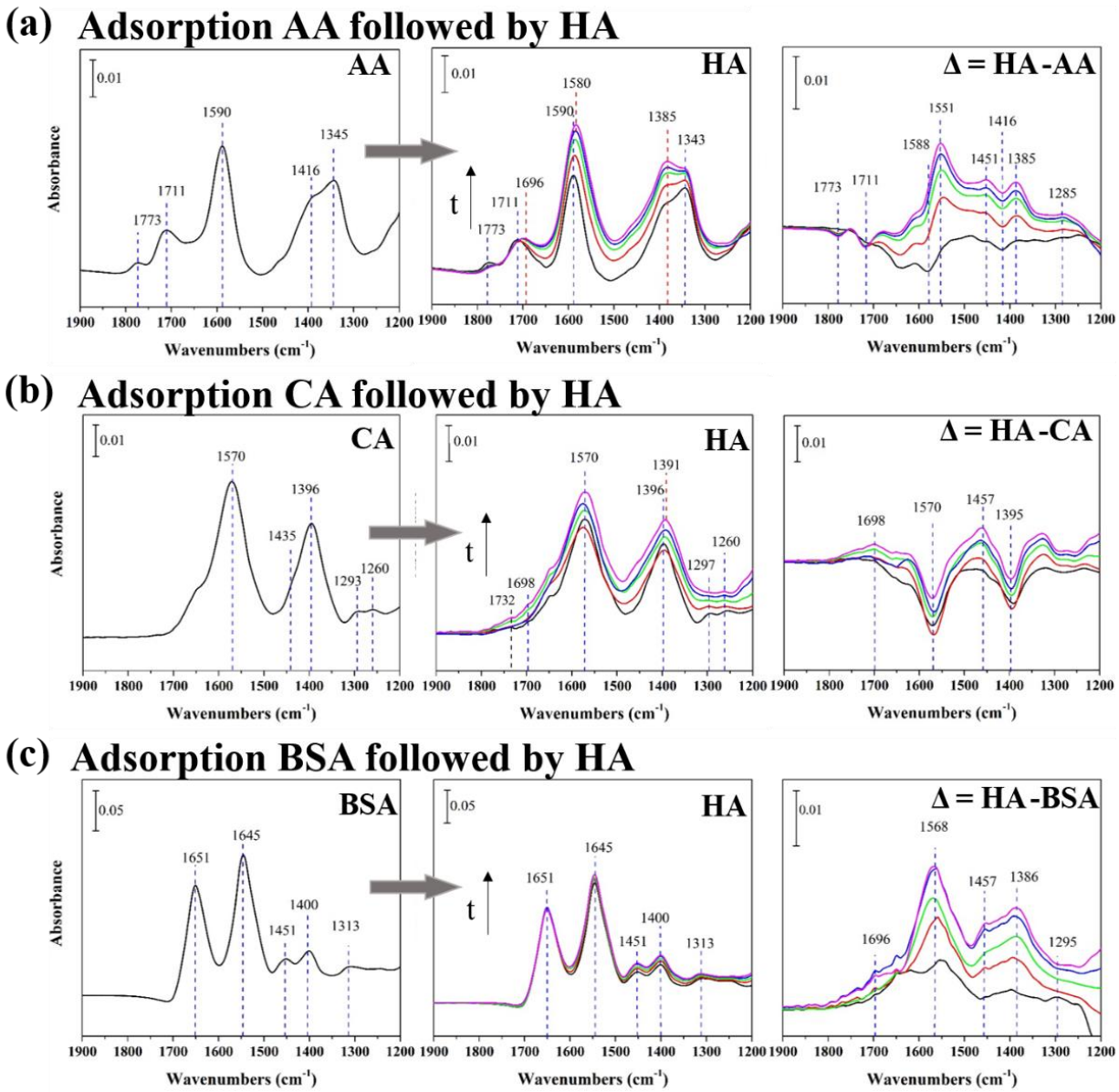

Figure 4. ATR-FTIR of the displacement reactions of AA-(a), CA-(b), and BSA-(c) pre-coated TiO_2 NPs by HA. The initial coating spectra are on the left, the time dependent displacement spectra are in the middle, and the difference spectra are on the right. The displacement spectra were collected at 5 min (black), 30 min (red), 60 min (green), 90 (blue), 120 min (magenta). The difference spectra were obtained by subtracting the initial spectra from displacement spectra.

introducing 0.05 g/L HA solution on the TiO_2 NP film that was pre-coated with AA, CA, and BSA

in the adsorption process, respectively. As seen in Figure 4a, the profile of the AA-coated TiO_2 NP spectra significantly changes during the displacement process. The main adsorption band shifts from 1590 to 1580 cm^{-1} when introducing HA to the TiO_2 film, and the other main adsorption band at 1385 cm^{-1} increases during the displacement process (Figure 4a middle). In addition, the band shifts from 1711 cm to 1696 cm^{-1} which is assigned to carbonyl vibration from HA. To confirm the presence of HA on the surface, the initial spectrum was subtracted from the displacement spectra, shown in Figure 4a right. The progressive decrease in time for the bands at 1773 and 1711 cm^{-1} from carbonyl vibrations due to adsorbed AA, indicates HA displaces AA. Also, two new peaks appear at 1551 and 1385 cm^{-1}, which correspond to the $–COO^-$ vibrations of HA. In addition, the asymmetric vibration of $–COO^-$ of HA appears to be shifted to 1551 cm^{-1} instead of 1570 cm^{-1} due to a negative contribution of the peak at 1590 cm^{-1} caused by the displacement. The absorption at 1285 cm^{-1} comes mainly from the deformation of –COO–Ti moiety when binding on the surface. All these changes indicate that HA displaces AA from the surface. Due to the reversible nature of the AA adsorption onto the TiO_2 surface, we hypothesize that HA displaces most of the AA as shown in the scheme in Figure 5a. However, it is not possible to rule out that some AA molecules are still attached on the surface.

During the displacement of CA, the similarity between carboxylate vibrations are the characteristic IR bands of CA (Figure 4b left), and these IR features are very similar to the vibrations observed for HA on TiO_2 surface (Figure 1d), which makes it difficult to discern the displacement process. However, during the displacement reaction (Figure 4b middle), it is seen that the symmetric stretching of COO– band at around 1396 cm^{-1} has around a 5 cm^{-1} red shift, changing from 1396 to 1391 cm^{-1}. In addition, the growing band above 1700 cm^{-1} is from the C=O of carboxylic acid group in HA. Furthermore, the difference spectra (Figure 4b right) corroborates

the displacement on TiO_2 NPs as it displays the main features of adsorbed HA onto TiO_2 NPs, such as carbonyl vibration from HA at 1698 cm^{-1}. Additionally, the main bands of CA at 1570 and 1395 cm^{-1} display growing negative values with time in the difference spectra, suggesting the loss of CA from the surface followed by a time dependent HA adsorption. Therefore, we infer that CA is partially displaced by HA as shown in Figure 5b. As suggested in the displacement process, when TiO_2 NPs fully coated with small molecules e.g. AA and CA are exposed to HA solution, HA tends to displace the pre-coatings. In the case of CA, it is possible that a partial displacement occurs as shown in Figure 5b, where HA displaces more weakly bonded CA molecules while co-adsorbing with CA which may be on edge and/or corner sites leading to more strongly bonded CA molecules on the surface of TiO_2 NPs.

In the case of BSA, the displacement process in Figure 4c (middle panel) shows no significant alteration of vibrational frequency, but an increase of intensity after introducing HA. The difference spectra (Figure 4c right) confirm that HA is adsorbing on the surface. A possible explanation is that HA mainly co–adsorbs with BSA rather than displaces it. At neutral pH, due to negative charges on both BSA and HA, electrostatic repulsion is expected, it is therefore concluded

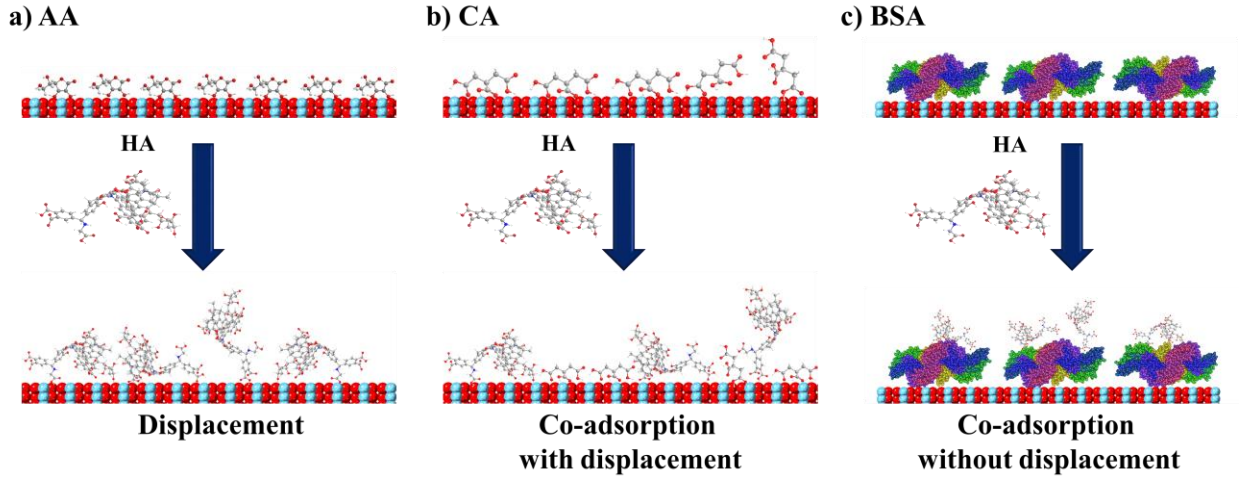

Figure 5. A schematic representation of displacement reactions and co-adsorption by HA on pre-coated TiO_2 surfaces with AA (a), CA (b), and BSA (c), respectively. HA is represented here as a macromolecular structure.

that non-specific hydrophobic interactions are the driving force for the co-adsorption of HA and BSA.[92-94] As Zhao *et al.* report,[92] HA can overlap on the top of BSA ring-like aggregates. Figure 5c shows both adsorption modes whereby HA stacks on top of the adsorbed BSA. In addition to ATR-FTIR study, the process of displacement of BSA by HA was also studied by QCM-D (Figure S4). Compared to BSA, HA has much lower molecular mass, therefore, if BSA was completely displaced by HA, the mass should decrease. However, the QCM-D result shows that the mass increases when introducing HA and the dissipation quickly reaches a value above two. This all supports that HA is not able to displace BSA but instead co-adsorb on the surface forming a second layer interacting with mainly adsorbed BSA molecules.

To corroborate the proposed displacement modes in Figure 5, the reverse processes were also investigated. In these experiments, NP surfaces were coated first with HA, then AA, CA or BSA was introduced and finally the buffer was flowed over the film after the displacement process. The spectra for each step are shown in Figure S5. The results agree with the expectation that AA weakly binds to the surface and no big change was observed after flowing buffer, therefore AA does not change or displace the HA-coating on the surface. CA is partially able to displace HA as reflected in the shift of the carboxylate symmetric vibration from 1385 to 1395 cm^{-1} corroborating that CA and HA are co-adsorbed. Most interesting is that BSA fully displaces HA from surface due to its strong binding ability. The summary of these processes is represented in Figure S6.

Due to the overlap of some IR bands in the one-dimensional spectra, 2D-COS was employed to investigate the details of the displacement of these initial molecular and protein coatings by HA. In addition, the synchronous (Φ) and asynchronous (Ψ) 2D correlation spectral maps are helpful in discerning the role of the functional groups in these displacement reactions. The synchronous

(left) and asynchronous (right) 2D correlation maps shown in Figure 6 are for the displacement by HA of NP surface pre-coated by AA (a), CA (b), and BSA (c), respectively.

When HA is introduced to the AA-coated TiO_2 NP film, three predominant autopeaks show up on the diagonal in synchronous 2D correlation spectra map (Figure 6a left) at near 1560, 1451 and 1386 cm^{-1}, which agree with the main bands in the HA spectra (Figure 1c), the positive values of the peaks indicate that the band intensity changes in the same direction. There is also a weak autopeak showing at 1277 cm^{-1}, which is assigned to δ(O=C-O-) when binding to TiO_2 surface.[52] Interestingly, there are a few barely noticeable small negative cross peaks appearing at (1560, 1775), (1560,1721), (1451, 1775), (1451, 1721), (1386, 1775), (1386, 1721). The negative peaks indicate that these band intensity changes are in opposite direction. During the displacement process, AA is displaced by HA, and HA adsorbs on surface, which results in a decrease of carbonyl from AA (1775 and 1721 cm^{-1}) and increase of carboxylate absorptions from HA (1560 and 1451 cm^{-1}). These data agree with the full surface displacement reaction proposed in Figure 5a. The asynchronous map (Figure 6a right) provides useful information of the sequential order of functional group changes in the adsorption. A series of cross peaks correlated to 1650 cm^{-1} assigned to C=O (ketone, amide) is observed, which merged into the peak of 1590 cm^{-1} in the 1D IR spectra. The relevant cross peaks in asynchronous map are positive, such as (1650, 1560), (1650, 1389), (1650, 1291), (1743, 1560), (1743, 1389), (1560, 1291) (1560, 1269). According to Noda's rules,[95] the main bands changes shown in the asynchronous map follow such order: 1743, 1650 cm^{-1} bands are prior to 1560 and 1389 cm^{-1}. This is followed by 1291 and 1269 $cm^{-1.}$ It indicates changes are in the sequence C=O (carboxylic) and C=O (ketone, amide) are earlier than COO^-, which is followed by COO–Ti (monodentate) and C–O–Ti (phenolic).

In the case of the CA-coated TiO_2 NP surface, when introducing HA, the synchronous map (left panel in Figure 6b) displays similar autopeaks to AA-coated surface at 1560, 1457 and 1372 cm^{-1}. In addition, two weak autopeaks were observed at 1696 and 1274 cm^{-1}, which are carbonyl

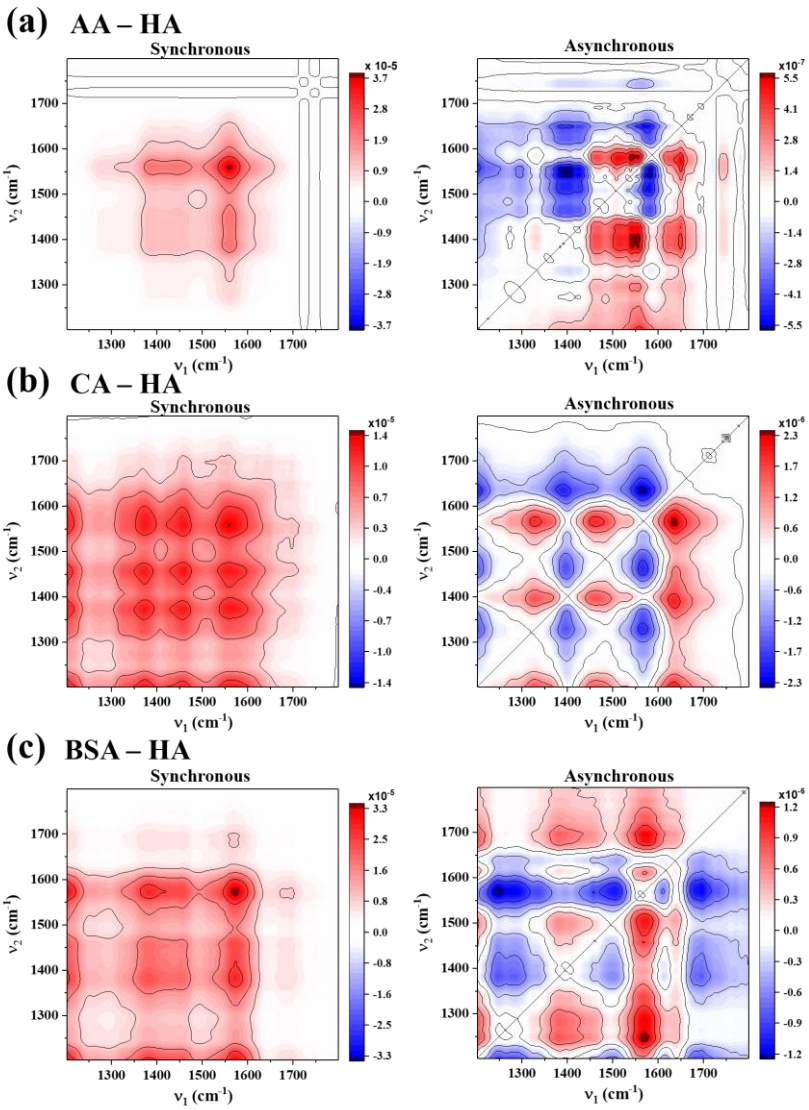

Figure 6. Synchronous (left) and asynchronous (right) 2D correlation maps following introduction of HA to a TiO_2 surface covered with (a) AA, (b) CA, and (c) BSA.

vibration and deformation of carboxylate from HA, respectively. The lack of negative peaks suggest that co-adsorption is the main process during the time-dependent reaction as proposed in

Figure 5b. The relevant cross peaks in asynchronous map are positive, such as (1638, 1560), (1638, 1390), (1638, 1460), (1696, 1560), (1696, 1460), (1330, 1560), (1330, 1390), (1460, 1560) (1330, 1264). This asynchronous map (Figure 6b right) exhibits a slightly different order: 1696, 1638 → 1460, 1330 →1560, 1390, 1264 cm^{-1}. The structural changes implied in asynchronous map follow such a sequence: C=O (carboxylic) and C=O (amide, ketone) are earlier than $COO^-$and C–O–Ti (phenol).

In comparison to the small molecules coated NPs, BSA-coated NPs has two main autopeaks (Figure 6c left) on the diagonal at 1572 and 1385 cm^{-1} representing the adsorption of HA. The lack of negative peaks supports the proposed co-adsorption scheme in Figure 5c. The relevant cross peaks in asynchronous map are positive, such as (1610, 1505), (1610,1250), (1570,1696), ((1570, 1505), (1570, 1284), (1505,1250). Based on the interpretation of the asynchronous 2D correlation map (Figure 6c right), the changes observed on the peaks during sorption follow the order 1570→ 1696, 1610 → 1505→ 1284, 1250 cm^{-1}. According to the sequence, the structural changes occur in this sequence: COO^- → C=O (amide, ketone) → C=C→ COO^- (bending), C–OH (phenol). Therefore, HA approaches BSA-coated TiO_2 surface through intermolecular interaction of H–bonding between these dangling functional groups (COO^- and C=O). As already noted, in the displacement reaction HA co-adsorbs on the surface mainly through interacting with BSA instead of displacing BSA. It has been reported that HA tends to interact with BSA ring-like aggregates by hydrophobic interaction,[92] thus resulting in the change of C=C vibration. The changes in the bending of carboxylate (1284 cm^{-1}) and the phenol vibration (1250 cm^{-1}) that show up after the changes in the C=C vibration also suggest that HA keeps changing conformation when adsorbing onto the BSA-coated TiO_2, this agrees with the changes on dissipation observed with QCM-D (Figure S4).

Chen *et al.* demonstrate that functional groups changes of HA while adsorbing onto bare TiO_2 follow the trend: carboxylate → C–O (phenol or tertiary) → C=O (ketone, amide) at pH 7.[45] In our study, the surface is pre-coated by other adsorbates and it is observed that HA shows a different adsorption pathway for each case compared to adsorption onto the hydroxylated surface. Therefore, we demonstrated that surface coatings on NP surfaces can modify the behavior of exactly how NPs interact with NOM in the environment.

Sedimentation and Agglomeration. In order to evaluate the effect of these coatings and displacement reactions on NP agglomeration with HA, the agglomeration was assessed by following the changes in the hydrodynamic size of the agglomerates and their sedimentation behavior. Figure 7 shows sedimentation curves of the TiO_2 NP suspensions before and after ligand displacement. Any impact would be of great significance for the transport and fate of NPs in the environment.[96-97] Adsorbates on TiO_2 NPs such as AA and CA result in steric repulsion, thus inhibiting the agglomeration of TiO_2 suspensions.[52, 69, 72] Therefore, the stability of TiO_2 NPs coated by AA or CA shows an increase compared to bare hydroxylated TiO_2 NPs in HEPES buffer (Figure 7a,b). In comparison to AA and CA, HA carries more polar functional groups such as

phenol and carboxylate and has stronger steric hindrance.[44, 98] As expected, the sedimentation rates of the samples after displaced by HA became much slower than those capped with only small molecules. Besides, the hydrodynamic diameters of the agglomerates are reduced in the presence of HA with agglomerate size decreasing from 350 to 250 nm. However, BSA has a strong interaction with TiO_2 NPs and enhance the electrostatic repulsion of TiO_2 NPs, resulting in the high stability of TiO_2 suspension, shown in Figure 7c. Although the stability stays the same for BSA-coated NPs, the addition of HA causes an increase in the hydrodynamic diameters from ca. 275 to 600 nm. At pH 7.5, the ligands on the surface are negatively charged. Therefore, the repulsive force in between each particle promotes the stability of these NPs in aqueous suspensions.[44, 52, 71, 83]

Conclusions

The adsorption of different environmentally and biologically relevant molecules onto TiO_2 NP surfaces has been systematically investigated. The ATR-FTIR measurements show that different functional group such as phenol, carboxylate, and enediol are involved in the adsorption process.

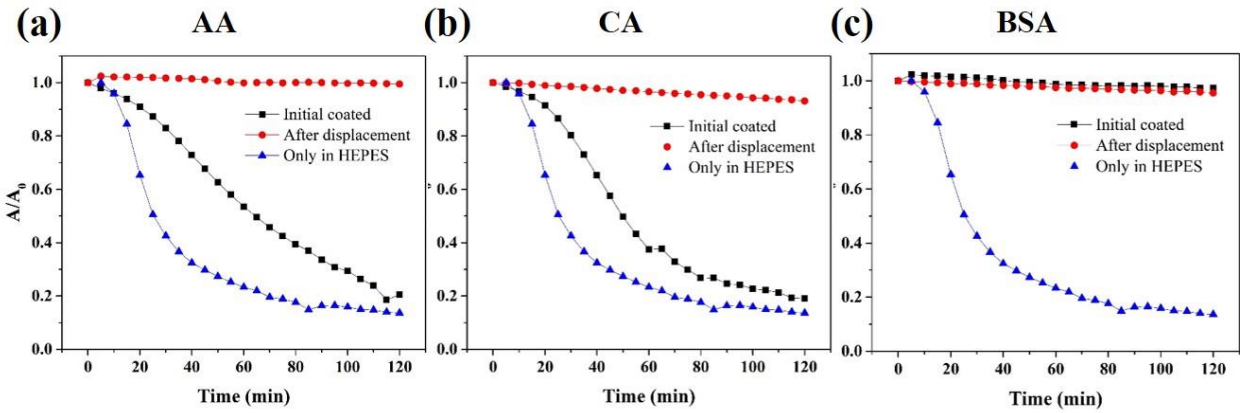

Figure 7. The effects of displacement reactions on sedimentation behavior of TiO_2NPs. The displacement reactions on the AA– (a), CA– (b) coated TiO_2 NPs with HA make the particles more stable (top) and smaller (bottom). However, HA is not able to displace BSA– (c) and it is shown not to affect the stability of the nanoparticle solution.

The desorption data suggest that under the conditions used in this study, AA and CA are able to reversibly and partially reversibly adsorb on TiO_2 surface, respectively. In contrast, BSA and HA mostly adsorb on the surface in an irreversible process monolayer, which is supported by the results from QCM-D. An interesting observation is that HA changes its conformation during adsorption process, reflected in the continuous increase of the dissipation. The properties of TiO_2 NPs are expected to be changed by NOM in the environment. Therefore, we focused on the displacement of different coatings on TiO_2 NPs with HA as it is a model for NOM found in the environment. Based on our study, the interaction between the small molecules and the surfaces of nanomaterials is reversible and HA can easily displace these molecules either fully or partially. However, the protein coated NPs shows no displacement but instead co-adsorbs with HA. Along with different coated TiO_2 NPs, 2D-COS provides relevant insights on the mechanism for the displacement reactions. In general, HA interacts with coated molecules first by weak interaction e.g. H-bonding and displaces these molecules by forming strong bonds with phenol and carboxylate groups. The effects of displacement reactions on sedimentation and agglomeration were studied. The results show that TiO_2 NPs with different coatings displayed a slower sedimentation rate in presence of HA. The hydrodynamic diameters of TiO_2 NPs were also modified by HA. These all imply that NOM can stabilize released NPs and influence the fate of NPs in the environment. The study shows not only the effect of NOM on sedimentation and agglomeration of coated NPs but also provides a first look on how displacement reactions may occur in the environment.

Acknowledgements. This material is based on the work supported by the National Science Foundation under grant number CHE1606607. This work was performed in part at the San Diego Nanotechnology Infrastructure (SDNI) of UCSD, a member of the National Nanotechnology Coordinated Infrastructure, which is supported by the National Science Foundation (Grant ECCS-

1542148). Any opinions, findings, and conclusions or recommendations expressed in this material are those of the authors and do not necessarily reflect the views of the National Science Foundation.

Electronic Supplementary Information (ESI). Supporting information includes additional experimental details and additional experimental data including the following figures: Figure S1 - morphology and phase of characterization data for TiO_2 NPs used; Figure S2 - characterization of NP thin film; Figure S3 - XPS data for QCM sensors; Figure S4 - changes in frequency and dissipation during the displacement process of BSA by HA onto a TiO_2 coated surface with QCM–D; Figure S5 – displacement reactions on HA pre-coated TiO_2 NPs through ATR-FIR by AA, CA, and BSA, respectively; Figure S6 – schematic of displacement processes on HA pre-coated TiO_2 NPs by AA, CA, and BSA, respectively.

References

1. Zhou, Q.; Zhong, Y. H.; Chen, X.; Liu, J. H.; Huang, X. J.; Wu, Y. C., Adsorption and photocatalysis removal of fulvic acid by TiO_2–graphene composites. *J. Mater. Sci.* **2014,** *49*, 1066-1075.

2. Dolamic, I.; Bürgi, T., In situ ATR-IR study on the photocatalytic decomposition of amino acids over Au/TiO_2 and TiO_2. *J. Phys. Chem. C.* **2011,** *115*, 2228-2234.

3. Jose, R.; Thavasi, V.; Ramakrishna, S., Metal oxides for dye-sensitized solar cells. *J. Am. Ceram. Soc.* **2009,** *92*, 289-301.

4. Jang, H. D.; Kim, S. K.; Chang, H.; Roh, K. M.; Choi, J. W.; Huang, J. x., A glucose biosensor based on TiO_2–Graphene composite. *Biosens. Bioelectron.* **2012,** *38*, 184-188.

5. Olariu, C. I.; Yiu, H. H. P.; Bouffier, L.; Nedjadi, T.; Costello, E.; Williams, S. R.; Halloran, C. M.; Rosseinsky, M. J., Multifunctional Fe_3O_4 nanoparticles for targeted bi-modal imaging of pancreatic cancer. *J. Mater. Chem.* **2011,** *21*, 12650-12659.

6. Javed, K. R.; Ahmad, M.; Ali, S.; Butt, M. Z.; Nafees, M.; Butt, A. R.; Nadeem, M.; Shahid, A., Comparison of doxorubicin anticancer drug loading on different metal oxide nanoparticles. *Medicine* **2015,** *94*, e617.

7. Sharma, H.; Kumar, K.; Choudhary, C.; Mishra, P. K.; Vaidya, B., Development and characterization of metal oxide nanoparticles for the delivery of anticancer drug. *Artif. Cells Blood Substit. Biotechnol.* **2016,** *44*, 672-679.

8. Garner, K. L.; Suh, S.; Keller, A. A., Assessing the risk of engineered nanomaterials in the environment: development and application of the nanofate model. *Environ. Sci. Technol.* **2017,** *51*, 5541-5551.

9. Feng, X.; Yan, Y.; Wan, B.; Li, W.; Jaisi, D. P.; Zheng, L.; Zhang, J.; Liu, F., Enhanced dissolution and transformation of ZnO nanoparticles: the role of inositol hexakisphosphate. *Environ. Sci. Technol.* **2016,** *50*, 5651-5660.

10. Gankanda, A.; Cwiertny, D. M.; Grassian, V. H., Role of atmospheric CO_2 and H_2O adsorption on ZnO and CuO nanoparticle aging: formation of new surface phases and the impact on nanoparticle dissolution. *J. Phys. Chem. C.* **2016,** *120*, 19195-19203.

11. Ma, R.; Stegemeier, J.; Levard, C.; Dale, J. G.; Noack, C. W.; Yang, T.; Brown, G. E.; Lowry, G. V., Sulfidation of copper oxide nanoparticles and properties of resulting copper sulfide. *Environ. Sci. Nano.* **2014,** *1*, 347.

12. Ma, R.; Levard, C.; Marinakos, S. M.; Cheng, Y.; Liu, J.; Michel, F. M.; Brown, G. E.; Lowry, G. V., Size-controlled dissolution of organic-coated silver nanoparticles. *Environ. Sci. Technol.* **2012,** *46*, 752-759.

13. Sendra, M.; Yeste, M. P.; Gatica, J. M.; Moreno-Garrido, I.; Blasco, J., Homoagglomeration and heteroagglomeration of TiO_2, in nanoparticle and bulk form, onto freshwater and marine microalgae. *Sci. Total Environ.* **2017,** *592*, 403-411.

14. Hedberg, J.; Ekvall, M. T.; Hansson, L.-A.; Cedervall, T.; Odnevall Wallinder, I., Tungsten carbide nanoparticles in simulated surface water with natural organic matter: dissolution, agglomeration, sedimentation and interaction with Daphnia magna. *Environ. Sci. Nano.* **2017,** *4*, 886-894.

15. Smijs, T. G.; Pavel, S., Titanium dioxide and zinc oxide nanoparticles in sunscreens: focus on their safety and effectiveness. *Nanotechnol. Sci. Appl.* **2011,** *4*, 95-112.

16. Daghrir, R.; Drogui, P.; Robert, D., Modified TiO_2 for environmental photocatalytic applications: a review. *Ind. Eng. Chem. Res.* **2013,** *52*, 3581-3599.

17. Wang, Y.; Wang, Q.; Zhan, X.; Wang, F.; Safdar, M.; He, J., Visible light driven type II heterostructures and their enhanced photocatalysis properties: a review. *Nanoscale* **2013,** *5*, 8326-8339.

18. Marks, R.; Yang, T.; Westerhoff, P.; Doudrick, K., Comparative analysis of the photocatalytic reduction of drinking water oxoanions using titanium dioxide. *Water Res.* **2016,** *104*, 11-19.

19. Li, Z.; Yang, R.; Yu, M.; Bai, F.; Li, C.; Wang, Z. L., Cellular level biocompatibility and biosafety of ZnO nanowires. *J. Phys. Chem. C.* **2008,** *112*, 20114-20117.

20. Ji, Z.; Jin, X.; George, S.; Xia, T.; Meng, H.; Wang, X.; Suarez, E.; Zhang, H.; Hoek, E. M. V.; Godwin, H.; Nel, A. E.; Zink, J. I., Dispersion and stability optimization of TiO_2 nanoparticles in cell culture media. *Environ. Sci. Technol.* **2010,** *44*, 7309-7314.

21. Ramani, M.; Mudge, M. C.; Morris, R. T.; Zhang, Y.; Warcholek, S. A.; Hurst, M. N.; Riviere, J. E.; DeLong, R. K., Zinc oxide nanoparticle–poly I:C RNA complexes: implication as therapeutics against experimental melanoma. *Mol. Pharm.* **2017,** *14*, 614-625.

22. Singh, S.; D'Britto, V.; Bharde, A.; Sastry, M.; Dhawan, A.; Prasad, B. L. V., Bacterial synthesis of photocatalytically active and biocompatible TiO_2 and ZnO nanoparticles. *Int. J. Green Nanotechnol. Phys. Chem.* **2010,** *2*, 80-99.

23. Yang, Y.; Doudrick, K.; Bi, X.; Hristovski, K.; Herckes, P.; Westerhoff, P.; Kaegi, R., Characterization of food-grade titanium dioxide: the presence of nanosized particles. *Environ. Sci. Technol.* **2014,** *48*, 6391-6400.

24. Du, W.; Sun, Y.; Ji, R.; Zhu, J.; Wu, J.; Guo, H., TiO_2 and ZnO nanoparticles negatively affect wheat growth and soil enzyme activities in agricultural soil. *J. Environ. Monit.* **2011,** *13*, 822-828.

25. Ghosh, M.; Chakraborty, A.; Mukherjee, A., Cytotoxic, genotoxic and the hemolytic effect of titanium dioxide (TiO_2) nanoparticles on human erythrocyte and lymphocyte cells in vitro. *J. Appl. Toxicol.* **2013,** *33*, 1097-1110.

26. Fang, T.; Yu, L. P.; Zhang, W. C.; Bao, S. P., Effects of humic acid and ionic strength on TiO_2 nanoparticles sublethal toxicity to zebrafish. *Ecotoxicology* **2015,** *24*, 2054-2066.

27. Xiong, S.; Tang, Y.; Ng, H. S.; Zhao, X.; Jiang, Z.; Chen, Z.; Ng, K. W.; Loo, S. C. J., Specific surface area of titanium dioxide (TiO_2) particles influences cyto- and photo-toxicity. *Toxicology* **2013,** *304*, 132-140.

28. Zhou, Z.; Son, J.; Harper, B.; Zhou, Z.; Harper, S., Influence of surface chemical properties on the toxicity of engineered zinc oxide nanoparticles to embryonic zebrafish. *Beilstein. J. Nanotechnol.* **2015,** *6*, 1568-1579.

29. Praetorius, A.; Scheringer, M.; Hungerbühler, K., Development of environmental fate models for engineered nanoparticles—a case study of TiO_2 nanoparticles in the Rhine River. *Environ. Sci. Technol.* **2012,** *46*, 6705-6713.

30. Labille, J.; Feng, J.; Botta, C.; Borschneck, D.; Sammut, M.; Cabie, M.; Auffan, M.; Rose, J.; Bottero, J.-Y., Aging of TiO_2 nanocomposites used in sunscreen. dispersion and fate of the degradation products in aqueous environment. *Environ. Pollut.* **2010,** *158*, 3482-3489.

31. Van Ravenzwaay, B.; Landsiedel, R.; Fabian, E.; Burkhardt, S.; Strauss, V.; Ma-Hock, L., Comparing fate and effects of three particles of different surface properties: nano-TiO_2, pigmentary TiO_2 and quartz. *Toxicol. Lett.* **2009,** *186*, 152-159.

32. Gallego-Urrea, J. A.; Perez Holmberg, J.; Hassellov, M., Influence of different types of natural organic matter on titania nanoparticle stability: effects of counter ion concentration and pH. *Environ. Sci. Nano.* **2014,** *1*, 181-189.

33. Loosli, F.; Le Coustumer, P.; Stoll, S., Effect of natural organic matter on the disagglomeration of manufactured TiO_2 nanoparticles. *Environ. Sci. Nano.* **2014,** *1*, 154-160.

34. Domingos, R. F.; Tufenkji, N.; Wilkinson, K. J., Aggregation of titanium dioxide nanoparticles: role of a fulvic acid. *Environ. Sci. Technol.* **2009,** *43*, 1282-1286.

35. Chowdhury, I.; Cwiertny, D. M.; Walker, S. L., Combined factors influencing the aggregation and deposition of nano-TiO_2 in the presence of humic acid and bacteria. *Environ. Sci. Technol.* **2012,** *46*, 6968-6976.

36. Domingos, R. F.; Rafiei, Z.; Monteiro, C. E.; Khan, M. A. K.; Wilkinson, K. J., Agglomeration and dissolution of zinc oxide nanoparticles: role of pH, ionic strength and fulvic acid. *Environ. Chem.* **2013,** *10*, 306-312.

37. Chen, G.; Liu, X.; Su, C., Distinct effects of humic acid on transport and retention of TiO_2 rutile nanoparticles in saturated sand columns. *Environ. Sci. Technol.* **2012,** *46*, 7142-7150.

38. Tang, W.-W.; Zeng, G.-M.; Gong, J.-L.; Liang, J.; Xu, P.; Zhang, C.; Huang, B.-B., Impact of humic/fulvic acid on the removal of heavy metals from aqueous solutions using nanomaterials: a review. *Sci. Total Environ.* **2014,** *468–469*, 1014-1027.

39. de Melo, B. A. G.; Motta, F. L.; Santana, M. H. A., Humic acids: structural properties and multiple functionalities for novel technological developments. *Materials Science and Engineering: C* **2016,** *62*, 967-974.

40. Kerndorff, H.; Schnitzer, M., Sorption of metals on humic acid. *Geochim. Cosmochim. Acta* **1980,** *44*, 1701-1708.

41. Hering, J. G.; Morel, F. M. M., Humic acid complexation of calcium and copper. *Environ. Sci. Technol.* **1988,** *22*, 1234-1237.

42. Yang, K.; Lin, D.; Xing, B., Interactions of humic acid with nanosized inorganic oxides. *Langmuir* **2009,** *25*, 3571-3576.

43. Sposito, G., *The surface chemistry of soils*. Oxford University Press: New York, 1984; p 234 pp.

44. Jayalath, S.; Wu, H.; Larsen, S. C.; Grassian, V. H., Surface adsorption of Suwannee River humic acid on TiO_2 nanoparticles: a study of pH and particle size. *Langmuir* **2018,** *34*, 3136-3145.

45. Chen, W.; Qian, C.; Liu, X.; Yu, H., Two-dimensional correlation spectroscopic analysis on the interaction between humic acids and TiO_2 nanoparticles. *Environ. Sci. Technol.* **2014,** *48*, 11119-11126.

46. Long, M.; Brame, J.; Qin, F.; Bao, J.; Li, Q.; Alvarez, P. J. J., Phosphate changes effect of humic acids on TiO_2 photocatalysis: from inhibition to mitigation of electron–hole recombination. *Environ. Sci. Technol.* **2017,** *51*, 514-521.

47. Drosos, M.; Ren, M.; Frimmel, F. H., The effect of NOM to TiO_2: interactions and photocatalytic behavior. *Appl. Catal. B* **2015,** *165*, 328-334.

48. Bian, S.-W.; Mudunkotuwa, I. A.; Rupasinghe, T.; Grassian, V. H., Aggregation and dissolution of 4 nm ZnO nanoparticles in aqueous environments: influence of pH, ionic strength, size, and adsorption of humic acid. *Langmuir* **2011,** *27*, 6059-6068.

49. Lin, D.; Ji, J.; Long, Z.; Yang, K.; Wu, F., The influence of dissolved and surface-bound humic acid on the toxicity of TiO_2 nanoparticles to Chlorella sp. *Water Res.* **2012,** *46*, 4477-4487.

50. Mudunkotuwa, I. A.; Grassian, V. H., Biological and environmental media control oxide nanoparticle surface composition: the roles of biological components (proteins and amino acids), inorganic oxyanions and humic acid. *Environ. Sci.: Nano* **2015,** *2*, 429-439.

51. Mudunkotuwa, I. A.; Minshid, A. A.; Grassian, V. H., ATR-FTIR spectroscopy as a tool to probe surface adsorption on nanoparticles at the liquid-solid interface in environmentally and biologically relevant media. *Analyst* **2014,** *139*, 870-881.

52. Mudunkotuwa, I. A.; Grassian, V. H., Citric acid adsorption on TiO_2 nanoparticles in aqueous suspensions at acidic and circumneutral pH: surface coverage, surface speciation, and its impact on nanoparticle−nanoparticle interactions. *J. Am. Chem. Soc.* **2010,** *132*, 14986-14994.

53. Bian, S. W.; Mudunkotuwa, I. A.; Rupasinghe, T.; Grassian, V. H., Aggregation and dissolution of 4 nm ZnO nanoparticles in aqueous environments: influence of pH, ionic strength, size, and adsorption of humic acid. *Langmuir* **2011,** *27*, 6059-68.

54. Mudunkotuwa, I. A.; Rupasinghe, T.; Wu, C.-M.; Grassian, V. H., Dissolution of zno nanoparticles at circumneutral pH: a study of size effects in the presence and absence of citric acid. *Langmuir* **2012,** *28*, 396-403.

55. Tsai, D.-H.; Davila-Morris, M.; DelRio, F. W.; Guha, S.; Zachariah, M. R.; Hackley, V. A., Quantitative determination of competitive molecular adsorption on gold nanoparticles using attenuated total reflectance–fourier transform infrared spectroscopy. *Langmuir* **2011,** *27*, 9302-9313.

56. Gonzalez-Pech, N. I.; Grassian, V. H., Surface chemical functionalities of environmental nanomaterials. In *Encyclopedia of Interfacial Chemistry: Surface Science and Electrochemistry*, Wandelt, K., Ed. Elsevier: 2018; pp 817-828.

57. Szeto, Y. T.; Tomlinson, B.; Benzie, I. F. F., Total antioxidant and ascorbic acid content of fresh fruits and vegetables: implications for dietary planning and food preservation. *Br. J. Nutr.* **2007,** *87*, 55-59.

58. Administration, U. S. F. a. D. *FDA investigations operations manual appendix C*; Washington, DC, 2015; pp 443-444.

59. Nasser, F.; Lynch, I., Secreted protein eco-corona mediates uptake and impacts of polystyrene nanoparticles on Daphnia magna. *Journal of Proteomics* **2016,** *137*, 45-51.

60. Schmidt, M. P.; Martínez, C. E., Kinetic and conformational insights of protein adsorption onto montmorillonite revealed using in situ ATR-FTIR/2D-COS. *Langmuir* **2016,** *32*, 7719-7729.

61. Noda, I., Generalized two-dimensional correlation method applicable to infrared, raman, and other types of spectroscopy. *Appl. Spectmsc.* **1993,** *47*, 1329-1336.

62. Noda, I., Two-dimensional infrared (2D IR) spectroscopy: theory and applications. *Appl. Spectmsc.* **1990,** *44*, 550-561.

63. Noda, I.; Ozaki, Y., Principle of two-dimensional correlation spectroscopy. In *Two-Dimensional Correlation Spectroscopy – Applications in Vibrational and Optical Spectroscopy*, John Wiley & Sons, Ltd: 2005; pp 15-38.

64. Baltrusaitis, J.; Jayaweera, P. M.; Grassian, V. H., Sulfur dioxide adsorption on TiO_2 nanoparticles: influence of particle size, coadsorbates, sample pretreatment, and light on surface speciation and surface coverage. *J. Phys. Chem. C.* **2011,** *115*, 492-500.

65. Reviakine, I.; Johannsmann, D.; Richter, R. P., Hearing what you cannot see and visualizing what you hear: Interpreting quartz crystal microbalance data from solvated interfaces. *Anal. Chem.* **2011,** *83*, 8838-8848.

66. Vogt, B. D.; Lin, E. K.; Wu, W.-l.; White, C. C., Effect of film thickness on the validity of the Sauerbrey equation for hydrated polyelectrolyte films. *J. Phys. Chem.B.* **2004,** *108*, 12685-12690.

67. Sauerbrey, G., Verwendung von Schwingquarzen zur Wägung dünner Schichten und zur Mikrowägung. *Z. Phys.* **1959,** *155*, 206-222.

68. Philippe, A.; Schaumann, G. E., Interactions of dissolved organic matter with natural and engineered inorganic colloids: a review. *Environ. Sci. Technol.* **2014,** *48*, 8946-8962.

69. Rajh, T.; Nedeljkovic, J. M.; Chen, L. X.; Poluektov, O.; Thurnauer, M. C., Improving optical and charge separation properties of nanocrystalline TiO_2 by surface modification with vitamin C. *J. Phys. Chem.B.* **1999,** *103*, 3515-3519.

70. Xagas, A. P.; Bernard, M. C.; Hugot-Le Goff, A.; Spyrellis, N.; Loizos, Z.; Falaras, P., Surface modification and photosensitisation of TiO_2 nanocrystalline films with ascorbic acid. *J. Photochem. Photobiol. A: Chem.* **2000,** *132*, 115-120.

71. Ou, Y.; Lin, J.-D.; Zou, H.; Liao, D., Effects of surface modification of TiO_2 with ascorbic acid on photocatalytic decolorization of an azo dye reactions and mechanisms. *J. Mol. Catal. A: Chem.* **2005,** *241*, 59-64.

72. Park, J.-W.; Shumaker-Parry, J. S., Structural study of citrate layers on gold nanoparticles: role of intermolecular interactions in stabilizing nanoparticles. *J. Am. Chem. Soc.* **2014,** *136*, 1907-1921.

73. Erhayem, M.; Sohn, M., Stability studies for titanium dioxide nanoparticles upon adsorption of Suwannee River humic and fulvic acids and natural organic matter. *Sci. Total Environ.* **2014,** *468–469*, 249-257.

74. Abrosimova, K. V.; Shulenina, O. V.; Paston, S. V., FTIR study of secondary structure of bovine serum albumin and ovalbumin. *J. Phys. Conf. Ser.* **2016,** *769*, 012016.

75. Turci, F.; Ghibaudi, E.; Colonna, M.; Boscolo, B.; Fenoglio, I.; Fubini, B., An integrated approach to the study of the interaction between proteins and nanoparticles. *Langmuir* **2010,** *26*, 8336-8346.

76. Xu, Z.; Grassian, V. H., Bovine serum albumin adsorption on TiO_2 nanoparticle surfaces: Effects of ph and coadsorption of phosphate on protein–surface interactions and protein structure. *J. Phys. Chem. C.* **2017,** *121*, 21763-21771.

77. Tsai, D.-H.; DelRio, F. W.; Keene, A. M.; Tyner, K. M.; MacCuspie, R. I.; Cho, T. J.; Zachariah, M. R.; Hackley, V. A., Adsorption and conformation of serum albumin protein on gold nanoparticles investigated using dimensional measurements and in situ spectroscopic methods. *Langmuir* **2011,** *27*, 2464-2477.

78. Dobson, K. D.; McQuillan, A. J., In situ infrared spectroscopic analysis of the adsorption of aliphatic carboxylic acids to TiO_2, ZrO_2, Al_2O_3, and Ta_2O_5 from aqueous solutions. *Spectrochim. Acta. A. Mol. Biomol. Spectrosc.* **1999,** *55*, 1395-1405.

79. Dobson, K. D.; McQuillan, A. J., In situ infrared spectroscopic analysis of the adsorption of aromatic carboxylic acids to TiO_2, ZrO_2, Al_2O_3, and Ta_2O_5 from aqueous solutions. *Spectrochim. Acta. A. Mol. Biomol. Spectrosc.* **2000,** *56*, 557-565.

80. Baes, A. U.; Bloom, P. R., Diffuse reflectance and transmission fourier transform infrared (DRIFT) spectroscopy of humic and fulvic acids. *Soil. Sci. Soc. Am. J.* **1989,** *53*, 695-700.

81. Yohannan Panicker, C.; Tresa Varghese, H.; Philip, D., FT-IR, FT-Raman and SERS spectra of vitamin C. *Spectrochim. Acta. A. Mol. Biomol. Spectrosc.* **2006,** *65*, 802-804.

82. Hvoslef, J.; Klæboe, P., Vibrational spectroscopic studies of L-ascorbic acid and sodium ascorbate. *Acta Chem. Scand.* **1971,** *25*, 3043-3053.

83. Márquez, A.; Berger, T.; Feinle, A.; Hüsing, N.; Himly, M.; Duschl, A.; Diwald, O., Bovine serum albumin adsorption on TiO_2 colloids: the effect of particle agglomeration and surface composition. *Langmuir* **2017,** *33*, 2551-2558.

84. Grdadolnik, J.; Maréchal, Y., Bovine serum albumin observed by infrared spectrometry. I. methodology, structural investigation, and water uptake. *Biopolymers* **2001,** *62*, 40-53.

85. Tajmir-Riahi, H. A., Coordination chemistry of vitamin C. Part I. interaction of L-ascorbic acid with alkaline earth metal ions in the crystalline solid and aqueous solution. *J. Inorg. Biochem.* **1990,** *40*, 181-188.

86. Berg, R. W., Investigation of L(+)-ascorbic acid with Raman spectroscopy in visible and UV light. *Applied Spectroscopy Reviews* **2015,** *50*, 193-239.

87. Eita, M., In situ study of the adsorption of humic acid on the surface of aluminium oxide by QCM-D reveals novel features. *Soft Matter* **2011,** *7*, 709-715.

88. Dixon, M. C., Quartz crystal microbalance with dissipation monitoring: Enabling real-time characterization of biological materials and their interactions. *Journal of Biomolecular Techniques : JBT* **2008,** *19*, 151-158.

89. Johannsmann, D., Viscoelastic, mechanical, and dielectric measurements on complex samples with the quartz crystal microbalance. *PCCP* **2008,** *10*, 4516-4534.

90. McNamara, T. P.; Blanford, C. F., A sensitivity metric and software to guide the analysis of soft films measured by a quartz crystal microbalance. *Analyst* **2016,** *141*, 2911-2919.

91. Zhang, B.; Wang, Q., Quartz crystal microbalance with dissipation. In *Nanotechnology research methods for foods and bioproducts*, Wiley-Blackwell: 2012; pp 181-194.

92. Zhao, J.; Wang, Z.; Ghosh, S.; Xing, B., Phenanthrene binding by humic acid–protein complexes as studied by passive dosing technique. *Environ. Pollut.* **2014,** *184*, 145-153.

93. Armanious, A.; Aeppli, M.; Sander, M., Dissolved organic matter adsorption to model surfaces: adlayer formation, properties, and dynamics at the nanoscale. *Environ. Sci. Technol.* **2014,** *48*, 9420-9429.

94. Tomaszewski, J. E.; Schwarzenbach, R. P.; Sander, M., Protein encapsulation by humic substances. *Environ. Sci. Technol.* **2011,** *45*, 6003-6010.

95. Noda, I.; Ozaki, Y., Practical computation of two-dimensional correlation spectra. In *Two-Dimensional Correlation Spectroscopy – Applications in Vibrational and Optical Spectroscopy*, John Wiley & Sons, Ltd: 2005; pp 39-46.

96. Nowack, B.; Bucheli, T. D., Occurrence, behavior and effects of nanoparticles in the environment. *Environ. Pollut.* **2007,** *150*, 5-22.

97. Godinez, I. G.; Darnault, C. J. G., Aggregation and transport of nano-TiO_2 in saturated porous media: effects of pH, surfactants and flow velocity. *Water Res.* **2011,** *45*, 839-851.

98. Li, S.; Sun, W., A comparative study on aggregation/sedimentation of TiO_2 nanoparticles in mono- and binary systems of fulvic acids and Fe(III). *J. Hazard. Mater.* **2011,** *197*, 70-79.

TOC Graphic

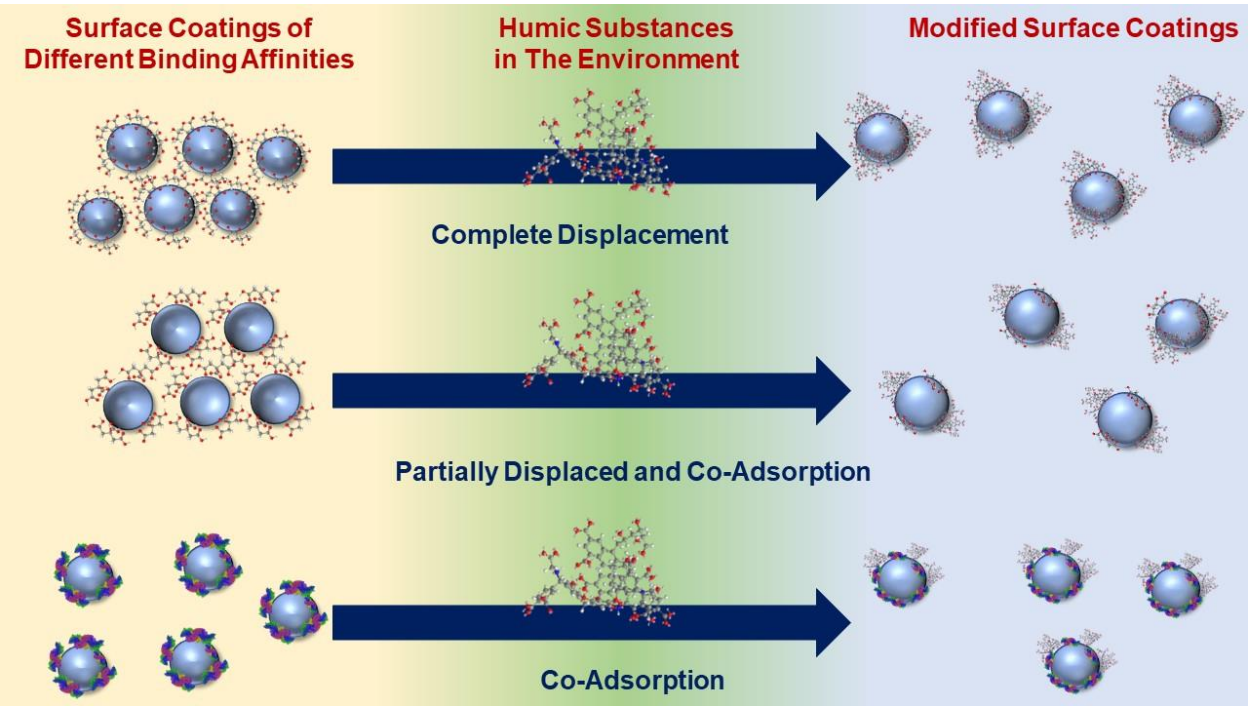
Surface Coatings of Different Binding Affinities
Humic Substances in The Environment
Modified Surface Coatings
Complete Displacement
Partially Displaced and Co-Adsorption
Co-Adsorption